Am J Cancer Res 2023;13(5):1884-1903
www.ajcr.us /ISSN:2156-6976/ajcr0149299

Original Article

High expression of peroxisomal D-bifunctional protein in cytosol regulates apoptosis and energy metabolism of hepatocellular carcinoma cells via PI3K/AKT pathway

Nan Zhang[1,2*], Ya-Qi Wang[1,3*], Chao Sun[4], Yun Shi[1], Lian-Guo Hou[1], Min Yao[1], Meng Hu[1,5], Xiao-Ming Wang[1,6], Pan-Pan Ma[7], Wen-Jie Li[8], Ling-Ling Jiang[1]

[1]Ministry of Education Key Laboratory of Neural and Vascular Biology, Department of Biochemistry and Molecular Biology, Hebei Medical University, Shijiazhuang, Hebei, China; [2]College of Integrative Chinese and Western Medicine, Hebei University of Chinese Medicine, Shijiazhuang, Hebei, China; [3]Department of Clinical Laboratory, Hebei Province Hospital of Chinese Medicine, Shijiazhuang, Hebei, China; [4]Department of Hepatobiliary Surgery, The Fourth Hospital of Hebei Medical University, Shijiazhuang, Hebei, China; [5]Department of Complex Preparation, Shijiazhuang No. 4 Pharmaceutical, Shijiazhuang, Hebei, China; [6]Department of Clinical Laboratory, The First Hospital of Tsinghua University, Beijing, China; [7]Department of Blood Transfusion, Hebei General Hospital, Shijiazhuang, Hebei, China; [8]Department of Clinical Laboratory, Anyang Center for Disease Control and Prevention, Anyang, Henan, China. [*]Equal contributors.

Received January 25, 2023; Accepted May 13, 2023; Epub May 15, 2023; Published May 30, 2023

Abstract: Peroxisomal D-bifunctional protein (DBP) is an indispensable enzyme of the fatty acid β-oxidation in the peroxisome of humans. However, the role of DBP in oncogenesis is poorly understood. Our previous studies have demonstrated that DBP overexpression promotes hepatocellular carcinoma (HCC) cell proliferation. In this study, we evaluated the expression of DBP in 75 primary HCC samples using RT-qPCR, immunohistochemistry, and Western blot, as well as its correlation with the prognosis of HCC. In addition, we explored the mechanisms by which DBP promotes HCC cell proliferation. We found that DBP expression was upregulated in HCC tumor tissues, and higher DBP expression was positively correlated with tumor size and TNM stage. Multinomial ordinal logistic regression analysis indicated that lower DBP mRNA level was an independent protective factor of HCC. Notably, DBP was overexpressed in the peroxisome and cytosol and mitochondria of tumor tissue cells. Xenograft tumor growth was promoted by overexpressing DBP outside peroxisome in vivo. Mechanistically, DBP overexpression in cytosol activated the PI3K/AKT signaling axis and promoted HCC cell proliferation by downregulating apoptosis via AKT/FOXO3a/Bim axis. In addition, overexpression of DBP increased glucose uptake and glycogen content via AKT/GSK3β axis, as well as elevated the activity of mitochondrial respiratory chain complex III to increase ATP content via the mitochondrial translocation of p-GSK3β in an AKT-dependent manner. Taken together, this study was the first to report the expression of DBP in peroxisome and cytosol, and that the cytosolic DBP has a critical role in the metabolic reprogramming and adaptation of HCC cells, which provides a valuable reference for instituting an HCC treatment plan.

Keywords: Peroxisomal D-bifunctional protein, hepatocellular carcinoma, HepG2, apoptosis, energy metabolism, PI3K/AKT pathway

Introduction

Peroxisomal D-bifunctional protein (DBP) is a D-3-hydroxyacyl-CoA dehydratase/D-3-hydroxyacyl-CoA dehydrogenase bifunctional enzyme with an SKL tripeptide (peroxisomal targeting signal type 1, PTS1) at C-terminus and ubiquitously expresses in human tissues. It catalyzes the second and third steps of the fatty acid β-oxidation in peroxisome and has an important role in the decomposition of very long-, polyunsaturated-, and branched-chain fatty acid, as well as in the synthesis of bile acid, plasmalogen, and docosahexaenoic acid (DHA). Studies have found that DBP defects can cause Zell-Weger-like syndrome, a severe congenital fatal disease with detrimental consequences on growth and development, due to peroxisome β-oxidation disorders [1] which leads to the degeneration of Purkinje cells [2]. Additionally,

DBP expression has been reported to be upregulated in several cancers, including prostate [3] and ovarian cancer [4]. In patients with prostate cancer, overexpression of DBP is associated with poor prognosis [3]. In addition, according to Human Protein Atlas (http://www.proteinatlas.org/ENSG00000133835/cancer/tissue/liver+cancer), liver cancer patients have higher levels of DBP protein in paraffin sections. Our previous studies have also demonstrated that DBP is upregulated in liver tissues of rat liver tumor model induced by 2-ethylnitrosamine (DEN) [5]. Moreover, DBP overexpression promotes the proliferation of HepG2 cells by activating several key oncogenic molecules such as AKT, STAT3, Cyclin D1, and PCNA [6]. However, as a protein in the peroxisome, the mechanisms underlying the growth-promoting function of DBP remains to be elucidated.

Material and methods

Reagents and antibodies

Phosphoinositide 3-kinase (PI3K) inhibitor LY294002 (GC15485; 20 mmol/L) and AKT inhibitor MK2206 (GC16304; 10 mmol/L) were purchased from GlpBio, New York, USA. Crystal violet (E607309) was purchased from Sangon Biotech, Shanghai, China and periodic acid-Schiff (PAS) (G1281) was purchased from Solarbio, Beijing, China.

The following antibodies were purchased from Cell Signaling Technology: Rabbit anti-p-AKT (4060), rabbit anti-AKT (4691S), rabbit anti-p-GSK3β (Ser9) (9323), mouse anti-GSK3β (9832), Rabbit anti-p-JNK (9251), rabbit anti-JNK (9252S), rabbit anti-COXIV (4850), rabbit anti-β-actin (8457), and HRP-conjugated anti-rabbit (7074S) or anti-mouse (7076S) antibody.

The following antibodies were purchased from Abcam: Rabbit anti-p-FOXO3a (ab26649) and rabbit anti-FOXO3a (ab23683).

The following antibodies were purchased from Proteintech: Rabbit anti-Bim (22037-1-AP), rabbit anti-LAMN (10298-1-AP), and rabbit anti-GAPDH (10494-1-AP).

The following antibodies were purchased from KPL, SareCare, Beijing XMJ Scientific Co.

Rhodamine-labeled antibody to rabbit IgG (031506), fluorescein-labeled antibody to mouse IgG (021815), rhodamine-labeled antibody to mouse IgG (031806) and fluorescein-labeled antibody to rabbit IgG (021516).

Mouse anti-DBP (sc-365167) was purchased from Santa Cruz Biotechnology while anti-PMP70 (PA1-650) was purchased from Invitrogen.

Tissue samples

Both liver tumor tissues and adjacent tissues (which were over 5 cm from tumor edges) were collected from HCC patients who underwent surgery at the Fourth Hospital of Hebei Province (Shijiazhuang, China). All samples were fixed for histochemistry staining and snap-frozen for further analysis. The HCC diagnosis was confirmed by two pathologists.

Cell culture and treatment with inhibitors

The human liver cancer HepG2 cells (cat. no. HB-8065; Manassas, VA, USA) were cultured in MEM medium supplemented with 10% FBS and penicillin and streptomycin (100 U/mL and 100 mg/mL, respectively) and were maintained in a humidified incubator at 37°C with 5% CO_2.

For inhibitor treatment, all inhibitors were dissolved in dimethyl sulfoxide (DMSO), and DMSO was used as vehicle control. Cells were treated for 2 h with phosphoinositide 3-kinase (PI3K) inhibitor LY294002 (20 mmol/L) or AKT inhibitor MK2206 (10 mmol/L).

Adenovirus expression vector construct and infection

cDNAs encoding DBP with peroxisomal targeting signal peptide SKL (DBP-SKL) or DBP with deletion of SKL (DBP-deSKL) were cloned into adenoviral vector, and adenovirus expressing DBP-SKL, DBP-deSKL, or empty vector (Empty) were produced by Sangon Biotech (Shanghai) Co., Ltd. HepG2 cells (5×10^6) were seeded in a six-well plate and cultured untill 40%-60% confluence. Then, cells were infected with adenovirus (5×10^9 PFU/mL) in serum-free medium for 36 h.

Small interfering RNA (siRNA) transfection

siRNAs specific to DBP and AKT as well as scramble siRNA were synthesized by Sangon Biotech. The sequences of these siRNAs were: siDBP: 5'-GUACCUUUGUAUUUGAGGAdTdT-3'

and 5'-UCCUCAAAUACAAAGGUACdTdT-3'; siAKT: 5'-GACGGGCACAUUAAGAUCATT-3' and 5'-UGAUCUUAAUGUGCCCGUCTT-3'; siNC: 5'-UUCUCCGAACGUGUCACGUTT-3' and 5'-ACGUGACACGUUCGGAGAATT-3'.

siRNA transfection was performed using the Lipofectamine 2000 reagent (Invitrogen) according to the manufacturer's instructions.

Reverse transcription-quantitative polymerase chain reaction (RT-qPCR)

Total RNA was extracted from HepG2 cells and the liver tissues of HCC patients using TRIzol reagent (Invitrogen, USA). cDNA was then synthesized using a SuperScript Reverse Transcription Kit (Invitrogen, USA) and used as a template for qPCR with SYBR Green fluorescence (Monad, Shanghai, China). Quantitative real-time PCR was run on an ABI 7500 Fast system (Life Technologies). 18S was used to normalize the RNA levels using the $2^{-\Delta\Delta}$ CT method [7]. Each experiment was conducted with three replicates. The primers were synthesized by Sangon Biotech, and their sequences were: DBP forward 5'-TTGGGCCGAGCCTATGC-3' and reverse 5'-CCCCTCCCAAATCATTCACA-3'; Bim forward 5'-AAGGTAATCCTGAAGGCAATCA-3' and reverse 5'-CTCATDBPGATGDBPAGCGGGG-3'; 18S forward 5'-CGCCGCTAGAGGTGDBPTTC-3' and reverse 5'-CCGGTCGGCATCGTTTATGG-3'.

Mitochondrial and nuclear protein isolation

Mitochondria were isolated from HepG2 cells using a Mitochondrion Isolation Kit (KGA827, KeyGEN BioTECH, China). Briefly, about 5×10^7 cells were homogenized in pre-cold lysis buffer and cleared by centrifugation at 1200 g at 4°C for 5 min to remove nuclei and cell debris. The supernatant was collected and centrifuged again at 7,000 g for 10 min at 4°C to precipitate mitochondria. The pellet was then resuspended in 3 ml respiration buffer and centrifuged at 9,500 g for 5 min at 4°C to reprecipitate mitochondria. The resulting pellet was resuspended in 50-100 µl Store Buffer, and the mitochondrial protein was qualified by Bradford method.

Nuclear proteins were extracted using the Nuclear Protein Extraction Kit (BB-3102, BestBio Corp., Shanghai, China). Briefly, the pellet of 5-10 × 10^6 cells was resuspended in cold Buffer A containing protease inhibitor mixture, vortexed at high speed every 5 minutes for 25 minutes and centrifuged at 12,000 g for 5 minutes at 4°C to precipitate nucleus, which was then resuspended in cold Buffer B to extract nuclear proteins. After centrifugation at 2,000 g for 10 minutes at 4°C, the supernatant containing nuclear protein was collected, and protein concentration was determined by Bradford method.

Western blot (WB)

Standard WB protocol was used in this study. Briefly, HepG2 cells or HCC liver tissues were lysed in RIPA buffer (Thermo Scientific, USA) with protease inhibitors, and protein concentration was determined by Bradford method. Proper exposure protein marker (G2086, Servicebio) and equal amounts of protein (30-50 µg) were separated by SDS-PAGE and transferred onto PVDF (Millipore, Ireland). Membranes were then blocked with 5% skimmed milk and incubated with the indicated primary antibodies at 4°C overnight. After extensive washing, the membranes were incubated with appropriate HRP-conjugated secondary antibody at room temperature for 1 h.

Enhanced chemiluminescence was used to detect the antibody-antigen complexes. Films were exposured from 3-5 minutes depending on the target protein to detect the chemiluminescence signal. Films were then developed and scanned using an Epson Perfection V39 scanner (Japan). Image conversion was performed using Adobe Photoshop software, while grayscale values were measured with Image J software. β-actin was used as a protein loading control.

Co-immunoprecipitation (Co-IP)

Briefly, HepG2 cells were lysed in RIPA buffer, and the cell lysates were subjected to IP with anti-DBP or anti-p-AKT antibodies, followed by incubation with protein A agarose beads. The precipitated complex was then washed with IPH buffer (50 mM Tris-HCl, pH 8.0, 150 mM NaCl, 5 mM EDTA, 0.5% NP-40, 0.1 mM PMSF) and resolved by SDS-PAGE, followed by WB with antibodies against DBP and p-AKT. The experiment was replicated three times.

Immunohistochemistry (IHC) staining

IHC staining was performed on the tissue section slides as previously described [8]. Briefly,

sections were blocked with goat serum and incubated with anti-DBP antibody. After extensive washing, the sections were incubated with the biotinylated secondary antibody, followed by incubation with HRP-streptavidin D. Then, the signal was developed using a diaminobenzidine kit (Zhongshan Goldenbridge Biotechnology, China) according to the manufacturer's instructions. Hematoxylin was used for nucleus counterstaining. Images were acquired using a Leica microscope (Leica DM6000B, LAS V.4.3, Switzerland). The number of positive cells was graded and scored by the number of positive chromogenic cells: 0-1% = 0, 1-10% = 1, 10-50% = 2, 50-80% = 3, and 80-100% = 4. The staining intensity was graded: 0 (negative), 1 (weakly positive), 2 (positive), and 3 (strongly positive). The immunohistochemistry score (IHS) was calculated using the following formula IHS = A × B, where A was the score for the percentage of stained cells, while B is the grade of staining intensity. The minimum score is 0, while the maximum score is 12. Immunohistochemical pictures were taken by Histo Faxs System. The average DAB staining intensity was calculated by HistoQuest software, which represented the relative protein level of DBP.

Immunofluorescence (IF) staining

Immunofluorescence staining was performed on 4-μm deparaffinized tissue sections from the liver of HCC patients and 4% paraformaldehyde-fixed HepG2 cells on glass slides. The slides were permeabilized by 1% Triton X-100 in PBS, blocked with 10% normal goat serum (710027, KPL, SareCare, Beijing XMJ Scientific Co.), and then incubated with the indicated antibodies at 4°C overnight. After washing, the slides were incubated with the corresponding secondary antibodies. The nuclei were counterstained with DAPI (157574, MP Biomedicals). Images were captured by confocal microscopy (DM6000 CFS, Leica), and the corresponding Pearson Correlation Coefficient (PCC) was calculated using the colocalization module of LAS AF software for relative quantification of colocalization [9].

Immunoelectron microscopy (IEM)

HepG2 cells were fixed with a mixture of 3% formaldehyde and 0.1% glutaraldehyde in 0.1 M cacodylate buffer, then sequentially dehydrated with 30%, 50%, and 100% ethanol, and embedded in LR Gold resin. Sections of 70 nm were cut and mounted on nickel grids, blocked with 1% BSA plus 5% normal goat serum (in PBS), and then incubated with a mouse anti-DBP in a humidified chamber at 4°C overnight. After flushing with PBS, the grids were incubated with the colloidal gold-labeled secondary antibody for 20 minutes at room temperature followed by incubation in a humidified chamber at 37°C for 1 h. Finally, the grids were washed with PBS and water, and the sections were stained with 2% uranyl acetate solution for 8 minutes in the dark. After washing with 70% alcohol and water, the grids were stored in the oven for further analysis. The ultrastructural distribution of DBP was examined and photographed with a Hitachi H-800 transmission electron microscopy. All experiments were repeated three times.

CCK-8 assay

Cell proliferation was measured using the CCK-8 kit (GK10001, GlpBio, America). Briefly, 1×10^4/100 μL cells were seeded into a well of 96-well plates in triplicate. CCK-8 solution was diluted with serum-free MEM medium at a ratio of 1:10. At the indicated time, the cell culture medium was replaced with 100 μL of diluted CCK-8 solution. After 1 h cultured, the optical density (OD) values at 450 nm were measured by a microplate reader (Thermo Scientific, USA). The experiment was repeated three times.

Colony formation assay

HepG2 cells were seeded into 6-well plates at 500 cells/well and cultured for 3 days, following by the corresponding treatment for 4 days. Then, cells were fixed with 4% paraformaldehyde solution for 10 minutes and stained with 0.1% crystal violet (E607309, Sangon Biotech) for 15 minutes. The number of colonies was counted under microscope. The experiment was replicated three times.

ATP assay

The intracellular ATP level was measured using ATP Assay Kit (Beyotime, Haimen, China). Briefly, HepG2 cells were lysed with ATP-releasing buffer, and the supernatants were collected by centrifugation at 12,000 g for 5 minutes. Then, 20 μl of the supernatants/given

concentration ATP was mixed with 100 μl ATP detection solution in a 96-well plate in triplicate. The luminescence signal was measured by a luminometer, and the protein concentration in the samples was measured by Bradford method. ATP level was expressed as nmol/mg protein. The experiment was replicated three times.

Apoptosis assay

Cell apoptosis was examined using an Annexin V FITC/PI Apoptosis Kit (MultiSciences, Hangzhou, China). Briefly, HepG2 cells were harvested and resuspended in 1 × binding buffer. Annexin V-FITC and PI were added to the cell suspension and incubated in the dark at room temperature. Early and late apoptotic cells were evaluated by flow cytometry (BD, United States). The experiment was replicated three times.

Periodic acid-schiff staining of tissue sections

Glycogen deposition in the liver tissues of patients was examined by periodic acid-Schiff (PAS) staining (Solarbio, G1281). Briefly, after dewaxing and rehydration, the liver tissue sections were stained with a periodic acid solution, washed in water, and then treated with Schiff solution. Following extensive rinsing with water, sections were counterstained with hematoxylin to visualize the nucleus. Glycogen deposition was observed under Microscope (Leica DM6000B, LAS V.4.3, Switzerland).

Glycogen measurement in cells

The glycogen level in cells was assessed using a glycogen assay kit (A043-1-1, Nanjing Jiancheng Bioengineering Institute, China) according to the manufacturer's protocol. Briefly, HepG2 cells were collected and sonicated in cold PBS. Protein concentration was determined by Bradford method. Then, the cell lysates were boiled in an alkali solution for 20 minutes followed by boiling in anthrone chromogenic solution for another 5 minutes. The optical density (OD) values were measured at 620 nm with a spectrophotometer. Glycogen level was expressed as mg/mg protein. The experiment was repeated three times.

Glucose uptake assay

The glucose uptake in HepG2 cells was assessed using 2-NBDG (Cayman). Briefly, HepG2 cells were cultured in a 96-well plate at a density of 1×10^4 cells/well and treated with 100 μmol/L of 2-NBDG in glucose and serum-free DMEM medium at 37°C for 30 minutes. The uptake of 2-NBDG by HepG2 cells was observed under a fluorescence microscope (Leica DM6000B, LAS V.4.3, Switzerland). After washing with PBS twice, the cells were used to measure fluorescence intensity at excitation and emission wavelengths of 488 and 520 nm.

Mitochondrial respiratory chain complexes III activity assay

The activity of mitochondrial respiratory chain complexes III in HepG2 cells was determined by measuring the reduction of cytochrome c at 550 nm with Mitochondrial Respiratory Chain Complex Activity Assay Kit (BC3240, Solarbio, Beijing, China). Briefly, 5×10^6 cells were homogenized in extraction solution and centrifuged at 600 g to remove the cell debris. The supernatant was centrifuged again at 11,000 g to precipitate mitochondria. The pellet was then sonicated in extraction solution to release the respiratory chain complexes III. After protein concentration (Cpr) measurement, 100 μl sample solution was used for the reduction reaction of cytochrome c. After the initial time and 2 min of the reaction, the absorbance at 550 nm was measured using a spectrophotometer, which was recorded as A1 and A2. The activity of mitochondrial respiratory chain complexes III was calculated as: Activity (U/mg prot) = 262 × (A2 - A1) ÷ Cpr.

Mouse xenograft tumor model

Male Balb/c nude mice (5 weeks old) were purchased from Beijing HFK Bioscience Co., Ltd. and housed in a pathogen-free barrier facility with a 12/12 h day/night cycle and free access to chow and water. To generate xenograft tumor, mice were randomly divided into Empty vector, DBP-SKL, or DBP-deSKL groups (n = 5/group) and were transplanted subcutaneously with 5×10^6 HepG2 cells expressing empty vector, DBP-SKL, or DBP-deSKL, respectively. Tumor growth was monitored, and at the 28 day post inoculation, the xenograft tumors were harvested and weighed. The tumor volume was calculated as $V = 0.5 \times \text{length} \times \text{width}^2$. The protocols using animals were approved by the ethical committee of Hebei University of Chinese Medicine and were conducted in Hebei University of Chinese Medicine.

Statistical analysis

All data were expressed as mean ± standard deviation (SD). SPSS 13.0 software was utilized for statistical analyses. The clinical properties between the high- and low-DBP mRNA expression groups were assessed with the Chi-Square test and Continuity Correction Chi-square test. Multivariable logistic regression analysis was performed to assess the association of DBP mRNA expression and the clinical properties with the TNM stage of HCC. Statistical differences between groups were assessed using a two-tailed Student's t-test or Wilcoxon signed-rank test. A value of $P<0.05$ was considered statistically significant. Diagrams were plotted using GraphPad Prism 5 software.

Results

DBP expression was upregulated in the tumor tissues of HCC patients and was positively associated with tumor size and TNM stage

To investigate the role of DBP in HCC progression, we evaluated the expression of DBP in HCC tumor tissues and the paired adjacent tissues. As shown in **Figure 1**, compared to the paired adjacent tissues, tumor tissues displayed significant increased mRNA (**Figure 1A**, P<0.001, n = 75) and protein levels as determined by WB (**Figure 1B**, P<0.001, n = 22) and by IHC staining (**Figure 1C**, IHC score: P<0.001, n = 54; average intensity: $P<0.001$, n = 20).

To determine the clinical significance of the upregulated DBP expression in HCC, we collected the clinical data from 75 patients with HCC and analyzed the relationship between DBP expression and the clinicopathological features. First, we divided these 75 patients into a high- (n = 58) and a low-DBP expression group (n = 17) using the average expression level of DBP mRNA in adjacent tissues ($2^{-\Delta Ct}$ = 0.005) as cut-off value according to Li et al. [10] and then compared the clinical characteristics between the two groups by Chi-Square test or Continuity Correction Chi-square test. As shown in **Table 1**, there was no significant difference in gender (P = 1.000), age (P = 0.971), alpha-fetoprotein (P = 0.773), alanine aminotransferase (P = 0.485), hepatitis B infection (P = 1.000), satellite nodules (P = 1.000), and lymphatic metastasis (P = 1.000) between the high- and low-expression groups. However, a significantly greater number of patients with larger tumors (>5 cm in diameter) (63.8% vs. 23.5%, P = 0.008) and more advanced TNM stage (III+IV) (74.2% vs. 41.2%, P = 0.011) were found in the high-DBP expression group than in the low-DBP expression group.

We also investigated the impact of DBP expression on the TNM stage of HCC patients by multinomial ordinal logistic regression. Patients were divided into four groups according to DBP mRNA level: mRNA≤0.005, 0.005< mRNA≤0.01, 0.01<mRNA≤0.02, and mRNA> 0.02. Because of the small sample size of patients with TNM IV, patients with I, II, and III+IV stages were analyzed. We found that, compared to those with higher TNM stages, patients with lower TNM stages showed no lymph node metastasis (OR = 0.172, 95% CI = 0.034-0.861, P = 0.032) and small tumor (<5 cm in diameters) (OR = 0.017, 95% CI = 0.004-0.079, P<0.001) as well as lower DBP mRNA level ≤0.02 (mRNA≤0.005, OR = 0.199, 95% CI = 0.045-0.883, P = 0.034; 0.005<mRNA≤ 0.01, OR = 0.134, 95% CI = 0.026-0.695, P = 0.017; 0.01<mRNA≤0.02, OR = 0.121, 95% CI = 0.024-0.614, P = 0.011) (**Table 2**). In contrast, gender (P = 0.171), age (P = 0.965), alpha-fetoprotein (AFP) (P = 0.268), alanine aminotransferase (ALT) (P = 0.603), hepatitis B infection (HBV) (P = 0.358) and satellite nodules (P = 0.245) were not significantly associated with the TNM stage of HCC. Together, these data suggested that DBP expression is upregulated and associated with tumor size and TNM stage of HCC.

Subcellular location of DBP in HCC tumor tissues

Furthermore, we assessed the subcellular localization of DBP in HCC tissues by IF staining. Images were sequentially taken using a confocal microscope, and the colocalization of DBP with a peroxisomal marker (PMP70), mitochondrial marker (COXIV), and cytosolic marker (GAPDH) was analyzed. DAPI staining showed that DBP was not localized in nuclei (**Figure 2A-C**). Instead, DBP was colocalized with PMP70 (PCC = 0.557±0.079) in peroxisome (**Figure 2A**), with COXIV (PCC = 0.467±0.082) in mitochondria (**Figure 2B**), and with GAPDH (PCC = 0.379±0.027) in cytosol (**Figure 2C**). In the paired adjacent tissues, DBP was also colo-

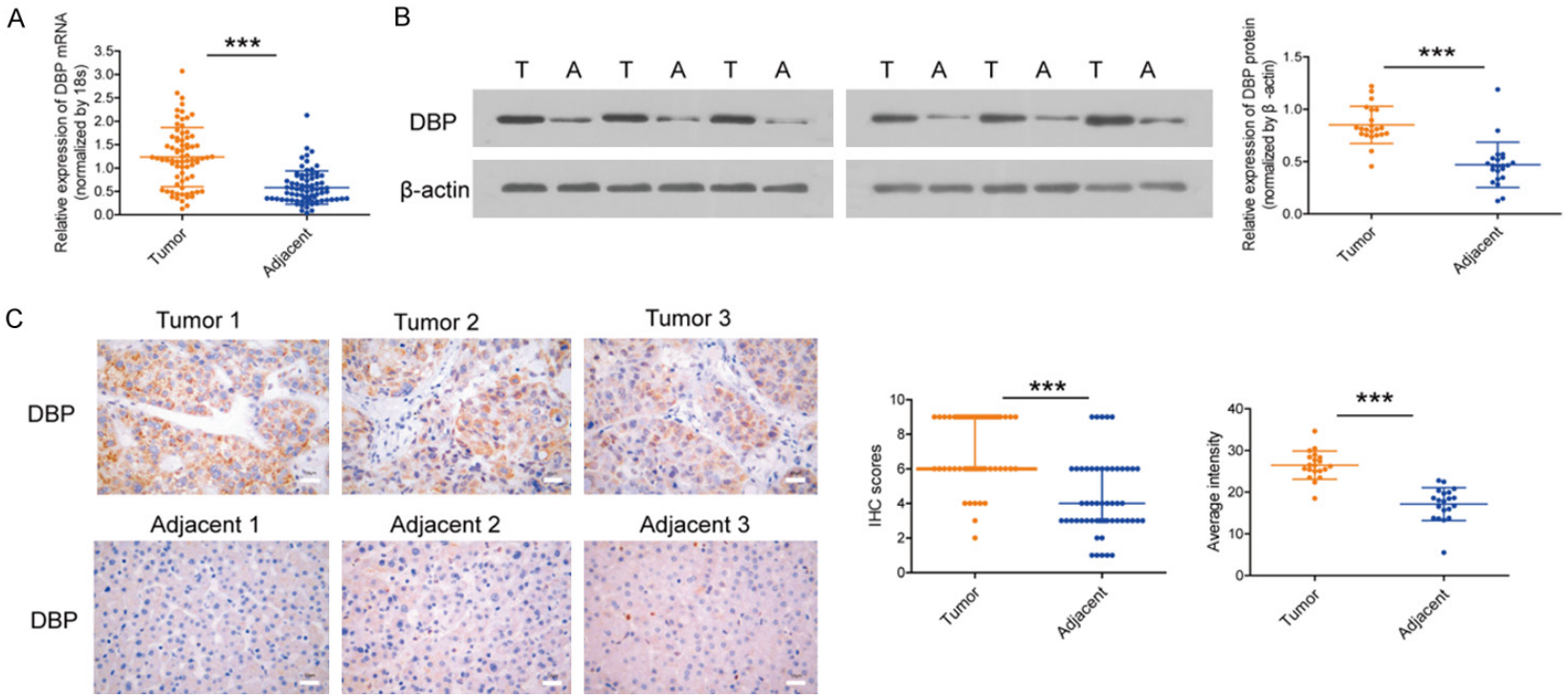

Figure 1. The expression of DBP in the liver tissues of human HCC. A. Relative expression of DBP mRNA in tumors and the adjacent liver tissues (n = 75 pairs). B. Representative WB images of DBP in tumors (T) and the adjacent (A) liver tissues. The corresponding quantitative data were presented (n = 22 pairs). C. Representative IHC staining images of DBP in tumors and the adjacent liver tissues. The corresponding staining intensities quantified by IHC score (n = 54 pairs) and by average intensity (n = 20 pairs) were shown. The staining of DBP expressed in cancer tissues varied from khaki to dark brown, and most of the DBP expression in the adjacent tissues was negative. Scale bars = 50 μm. Data of IHC scores were presented as median and interquartile range. Data of average intensity were presented as mean ± SD. ***P<0.001 vs. Tumor group.

Table 1. Comparison of the clinical properties between the high- and low-DBP mRNA expression groups

Clinical properties	DBP mRNA		χ^2	*P*
	High (≥0.005) (n = 58)	Low (<0.005) (n = 17)		
Gender (%)				
Male	47 (81.0%)	14 (82.4%)	0.000	1.000
Female	11 (19.0%)	3 (17.6%)		
Age (year)				
≤60	31 (53.4%)	9 (52.9%)	0.001	0.971
>60	27 (46.6%)	8 (47.1%)		
AFP (μg/L)				
≤400	25 (43.1%)	8 (47.1%)	0.083	0.773
>400	33 (56.9%)	9 (52.9%)		
ALT (U/L)				
≤40	32 (56.2%)	11 (64.7%)	0.488	0.485
>40	26 (43.8%)	6 (35.3%)		
HBV infection				
No	6 (10.4%)	2 (11.8%)	0.000	1.000
Yes	52 (89.6%)	15 (88.2%)		
Tumor size (cm)				
≤5	21 (36.2%)	13 (76.5%)	7.052	0.008
>5	37 (63.8%)	4 (23.5%)		
Satellite lesion				
No	41 (70.7%)	12 (70.6%)	0.000	1.000
Yes	17 (29.3%)	5 (29.4%)		
Lymph node metastasis				
No	51 (87.9%)	15 (88.2%)	0.000	1.000
Yes	7 (12.1%)	2 (11.8%)		
TNM staging				
I-II	15 (25.8%)	10 (58.8%)	6.427	0.011
III-IV	43 (74.2%)	7 (41.2%)		

Note: Statistically significant: *P*<0.05. Abbreviations: AFP: alpha-fetoprotein; ALT: alanine aminotransferase; HBV: hepatitis B infection.

calized with PMP70 (PCC = 0.371±0.075) (**Figure 2A**), COXIV (PCC = 0.174±0.091) (**Figure 2B**), and GAPDH (PCC = 0.181±0.080) (**Figure 2C**). However, the PCC values of DBP and PMP70, DBP and COXIV, and DBP and GAPDH in HCC tumor tissues were 1.50- (P<0.01), 2.68- (P<0.001), and 2.09-fold (P<0.001), respectively, higher than that of the adjacent tissues. Notably, the increase in the mitochondrial and cytosolic localization of DBP was more significant than that of peroxisomal DBP.

To further verify the subcellular location of the overexpressed DBP, we overexpressed DBP-SKL, DBP-deSKL, or empty vector in HepG2 cells by adenoviral infection (**Figure 2G**) and performed IF staining on them. Similarly, in the Empty vector group, DBP was colocalized with PMP70 (PCC = 0.482±0.098) (**Figure 2D**), COXIV (PCC = 0.213±0,034) (**Figure 2E**), and GAPDH (PCC = 0.257±0,034) (**Figure 2F**). In the DBP-SKL group, DBP was also colocalized with PMP70 (PCC = 0.635±0.033) (**Figure 2D**), COXIV (PCC = 0.452± 0.019) (**Figure 2E**), and GAPDH (PCC = 0.348±0.015) (**Figure 2F**). Nevertheless, the PCC values of DBP and PMP70, DBP and COXIV, and DBP and GAPDH in the DBP-SKL group were 1.31- (P<0.05), 2.12- (P<0.001), and 1.35-fold (P<0.01), respectively, higher than that of the Empty vector group, indicating that the localization of DBP in mitochondria was increased more than that in peroxisome and cytosol when DBP-SKL was overexpressed. Interestingly, in the DBP-deSKL group, although DBP was also colocalized with peroxisome PMP70 (PCC = 0.488±0.044) (**Figure 2D**), COXIV (PCC = 0.482±0.018 (**Figure 2E**), and GAPDH (PCC = 0.485±0.022) (**Figure 2F**), the PCC values of DBP and PMP70, DBP and COXIV, and DBP and GAPDH were 1.03 (P>0.05), 2.26 (P<0.001), and 1.88 fold (P<0.01), respectively, higher than that of the Empty vector group, suggesting a more significant increase of DBP in mitochondria and cytosol when DBP-deSKL was overexpressed. These results indicated that the DBP overexpressed in HCC may locate in peroxisome, as well as cytosol and mitochondria.

The mitochondrial localization of DBP was further studied by subcellular fractionation. HepG2 cells overexpressing DBP-SKL, DBP-deSKL, or empty vector were separated into the nuclear and mitochondrial fractions. The overexpression of DBP-SKL or DBP-deSKL was confirmed by WB (**Figure 2G**). Consistent with the results above, DBP-SKL or DBP-deSKL was not detected in the nuclear fraction but was present in the mitochondrial fraction (**Figure 2H**).

Table 2. Multivariate ordinal logistic regression analysis of the association of DBP mRNA expression and the clinical properties with the TNM stage of HCC

Variables	β value	OR value	95% CI	*P* value
mRNA				
mRNA≤0.005	-1.612	0.199	0.045-0.883	0.034
0.005<mRNA≤0.01	-2.010	0.134	0.026-0.695	0.017
0.01<mRNA≤0.02	-2.109	0.121	0.024-0.614	0.011
mRNA>0.02	0[a]	1		
Gender (%)				
Female	0.992	2.679	0.652-11.145	0.171
Male	0[a]	1		
Age (year)				
≤60	-0.024	0.976	0.335-2.849	0.965
>60	0[a]	1		
AFP (μg/L)				
≤400	-0.602	0.548	0.189-1.587	0.268
>400	0[a]	1		
ALT (U/L)				
≤40	-0.290	0.748	0.251-2.232	0.603
>40	0[a]	1		
HBV				
Positive	-0.817	0.442	0.077-2.524	0.358
Negative	0[a]	1		
Tumor size				
≤5 cm	-4.072	0.017	0.004-0.079	<0.001
>5 cm	0[a]	1		
Satellite lesion				
Negative	0.709	2.032	0.615-6.713	0.245
Positive	0[a]	1		
Lymph node metastasis				
Negative	-1.762	0.172	0.034-0.861	0.032
Positive	0[a]	1		

Note: Statistically significant: *P*<0.05. a: This parameter is set to zero because it is redundant. Abbreviations: AFP: alpha-fetoprotein; ALT: alanine aminotransferase; HBV: hepatitis B infection.

In addition, immunoelectron microscopy was performed to further verify the mitochondrial translocation of overexpressed DBP. As shown in **Figure 2I**, the DBP-SKL and DBP-deSKL groups had more DBP colloidal gold particles in mitochondria than the empty vector group did, in consistent with the results described above.

Overexpression of DBP with SKL or with SKL deletion promoted the growth of HCC xenograft tumor

Our previous study demonstrated that DBP in peroxisome promoted the growth of xenograft tumor in nude mice [11]. To investigate whether cytosol DBP could enhance tumor formation in vivo, we did xenograft assay in nude mice. As shown in **Figure 3A**, **3B**, cytosol DBP (DBP-deSKL group) could also significantly enhanced tumor formation in vivo (A). DBP expression in xenograft tumor tissues was higher in DBP-SKL and DBP-deSKL groups than the Empty group (B). Notably, weight (**Figure 3C**) and volume (**Figure 3D**) of xenograft were significantly increased in DBP-SKL and DBP-deSKL groups compared with that in the Empty vector group (P<0.001). Additionally, no obvious body weight loss was observed in mice after transplantation with treated HepG2 cells (**Figure 3E**). This observation suggested that DBP overexpression both in peroxisome and outside peroxisome promoted the malignant growth of subcutaneous carcinoma xenograft in nude mice.

Cytosolic DBP overexpression promoted the proliferation of HepG2 cells via PI3K/AKT/FOXO3a/Bim signaling pathway

To elucidate the mechanisms by which cytosolic DBP promotes cell proliferation, we explored the relationship between DBP and PI3K/AKT/FOXO3a/Bim pathway in the proliferation. First, we overexpressed DBP-SKL or DBP-deSKL in HepG2 cells to differentiate DBP activity in peroxisome or in cytosol. We also used siDBP to knockdown endogenous peroxisomal DBP. As shown in **Figure 4A**, while knocking down of DBP had no effect on the level of p-JNK, p-AKT and p-FOXO3a, overexpression of DBP-SKL or DBP-deSKL significantly enhanced the levels of p-AKT and p-FOXO3a, while there was no effect on p-JNK. In addition, the increased levels of p-AKT and p-FOXO3a were significantly attenated by treatment with the inhibitors of PI3K (LY294002) or AKT (MK2206), or by siAKT (**Figure 4A**, **4B**). These results suggest that increased DBP in cytosol could activate PI3K, leading to the increased phosphorylation of AKT and FOXO3a.

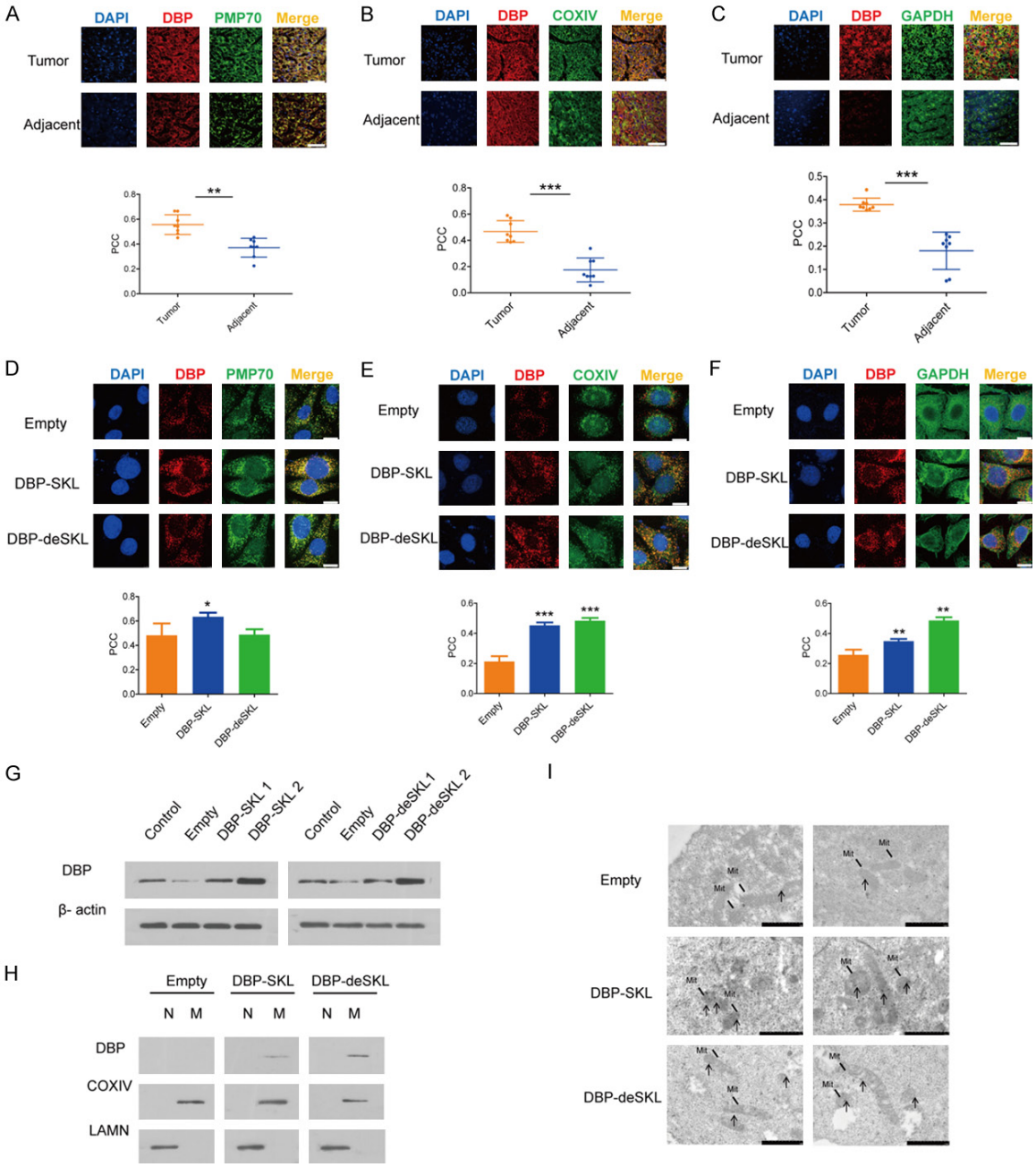

Figure 2. Subcellular location of DBP in human HCC tumor tissues, the adjacent tissues, and HepG2 cells. Quantitative PCC data were presented for each staining. (A-C) The IF images of DBP (red), nucleus (blue), and co-stained peroxisomal marker PMP70 (green) (A), mitochondrial marker COXIV (green) (B), and cytosolic marker GAPDH (green) (C) in HCC and adjacent tissues. Scale bar = 50 μm, magnification: 63X. (D-F) IF staining of HepG2 cells expressing DBP-SKL, DBP-deSKL, or Empty vector. IF images of DBP (red), PMP70 (green) (D), COXIV (green) (E), and GAPDH (green) (F). Scale bar = 10 μm. (G) WB of DBP in HepG2 cells expressing DBP-SKL, DBP-deSKL, or Empty vector. Control: parental cells. (H) WB of DBP in mitochondrial fraction (M, COXIV as marker) and nuclear fraction (N, LAMN as marker). (I) The immunoelectron microscopy images of HepG2 cells expressing DBP (Mit: mitochondria; arrow↑: DBP colloidal gold particles). HepG2 cells were infected with control adenovirus (Empty), adenovirus expressing DBP-SKL, or DBP-deSKL. Data were presented as mean ± SD. *P<0.05, **P<0.01 and ***P<0.001 vs. Empty or Tumor group.

Consistent with previous reports that the phosphorylated form of FOXO3a is localized in the cytosol [12, 13], our results showed that overexpression of DBP-SKL or DBP-deSKL resulted in a decreased level of nuclear FOXO3a (**Figure 4C**). As shown in **Figure 4D**, a weak colocaliza-

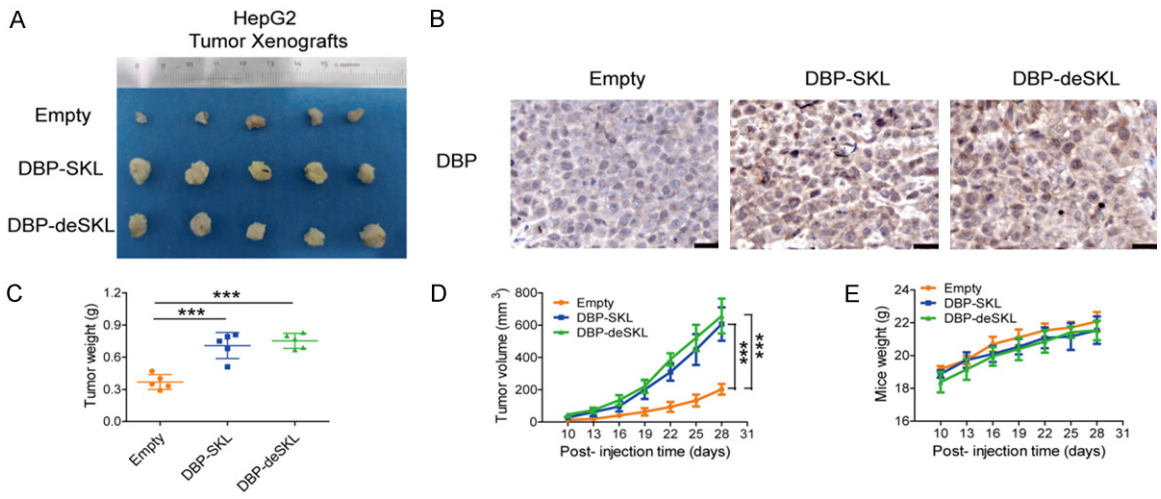

Figure 3. Overexpression of DBP with or without peroxisomal target peptide SKL increased the malignant growth of subcutaneous carcinoma xenograft in vivo. A. Images of subcutaneous tumors from mice implanted with HepG2 cells infected with Empty control adenovirus and DBP-SKL or DBP-deSKL overexpression adenovirus. B. Representative IHC staining images of DBP in the xenograft tumors from each group. Scale bars = 20 μm. C. Tumor weights when the mice were sacrificed. D. Tumor growth progression. E. Mice weight changes. n = 5/group. Data were presented as mean ± SD. ***P<0.001 vs. Empty group.

tion of FOXO3a and DAPI was observed in DBP-SKL group (n = 5; PCC = 0.437±0.052; P<0.001) and DBP-deSKL group (n = 5; PCC = 0.431±0.041; P<0.001) compared to that in the empty vector group (n = 5; PCC = 0.708±0.007), while MK2206 treatment could increase this colocalization in DBP-SKL+MK group (n = 5; PCC = 0.665±0.013; P<0.001) and in DBP-deSKL+MK group (n = 5; PCC = 0.648±0.046; P<0.001). Furthermore, we found that overexpression of DBP-SKL or DBP-deSKL downregulated the mRNA (P<0.01; **Figure 4E**) and protein (P<0.05; **Figure 4A**) levels of Bim, a downstream target gene of FOXO3a. Taken together, our data suggest that the cytosolic DBP could activate the PI3K/AKT/FOXO3a/Bim signaling pathway in HepG2 cells.

In addition, consistent with the downregulation of apoptosis-related Bim protein, we found that overexpression of DBP-SKL or DBP-deSKL inhibited apoptosis (P<0.05; **Figure 4F**) as well as increased cell viability (P<0.05; **Figure 4G**) and colony formation ability (P<0.01; **Figure 4H**). Conversely, treatment with inhibitor LY294002/MK2206 resulted in the opposite effects (**Figure 4F-H**).

Mitochondrial localization of DBP was p-AKT dependent

We further verified the localization of DBP in mitochondria when AKT is activated by PI3K. We speculated that the mitochondrial localization of DBP was likely related to the phosphorylation of DBP by AKT. To test this, we examined the phosphorylation level of DBP in HCC liver tissues and HepG2 cells. In addition, we also determined the effects of AKT inhibitor MK2206 on the subcellular localization of DBP in HepG2 cells and in the mitochondrial fraction, as well as the interaction between p-AKT and DBP.

As shown in **Figure 5A**, MK2206 did not affect the colocalization of PMP70 with DBP in DBP-SKL- (n = 5; $PCC_{DBP\text{-}SKL}$ = 0.631±0.021, $PCC_{DBP\text{-}SKL+MK2206}$ = 0.630±0.062, P>0.05) or DBP-deSKL-overexpressing group (n = 5; $PCC_{DBP\text{-}deSKL}$ = 0.481±0.040, $PCC_{DBP\text{-}deSKL+MK2206}$ = 0.501±0.034, P>0.05), suggesting that the peroxisomal localization of DBP was not p-AKT dependent. However, MK2206 reduced the colocalization of COXIV with DBP in DBP-SKL- (n = 5; $PCC_{DBP\text{-}SKL}$ = 0.441±0.017, $PCC_{DBP\text{-}SKL+MK2206}$ = 0.243±0.054, P<0.001) or DBP-deSKL-overexpressing group (n = 5; $PCC_{DBP\text{-}deSKL}$ = 0.442±0.020, $PCC_{DBP\text{-}deSKL+MK2206}$ = 0.303±0.025, P<0.001) (**Figure 5B**), suggesting that the mitochondrial localization of DBP was dependent on the phosphorylation of AKT. In contrast, MK2206 did not affect the colocalization of GAPDH with DBP in DBP-SKL- (n = 5; $PCC_{DBP\text{-}SKL}$ = 0.311±0.044, $PCC_{DBP\text{-}SKL+MK2206}$ = 0.320±0.071, P>0.05) or DBP-deSKL-overexpress-

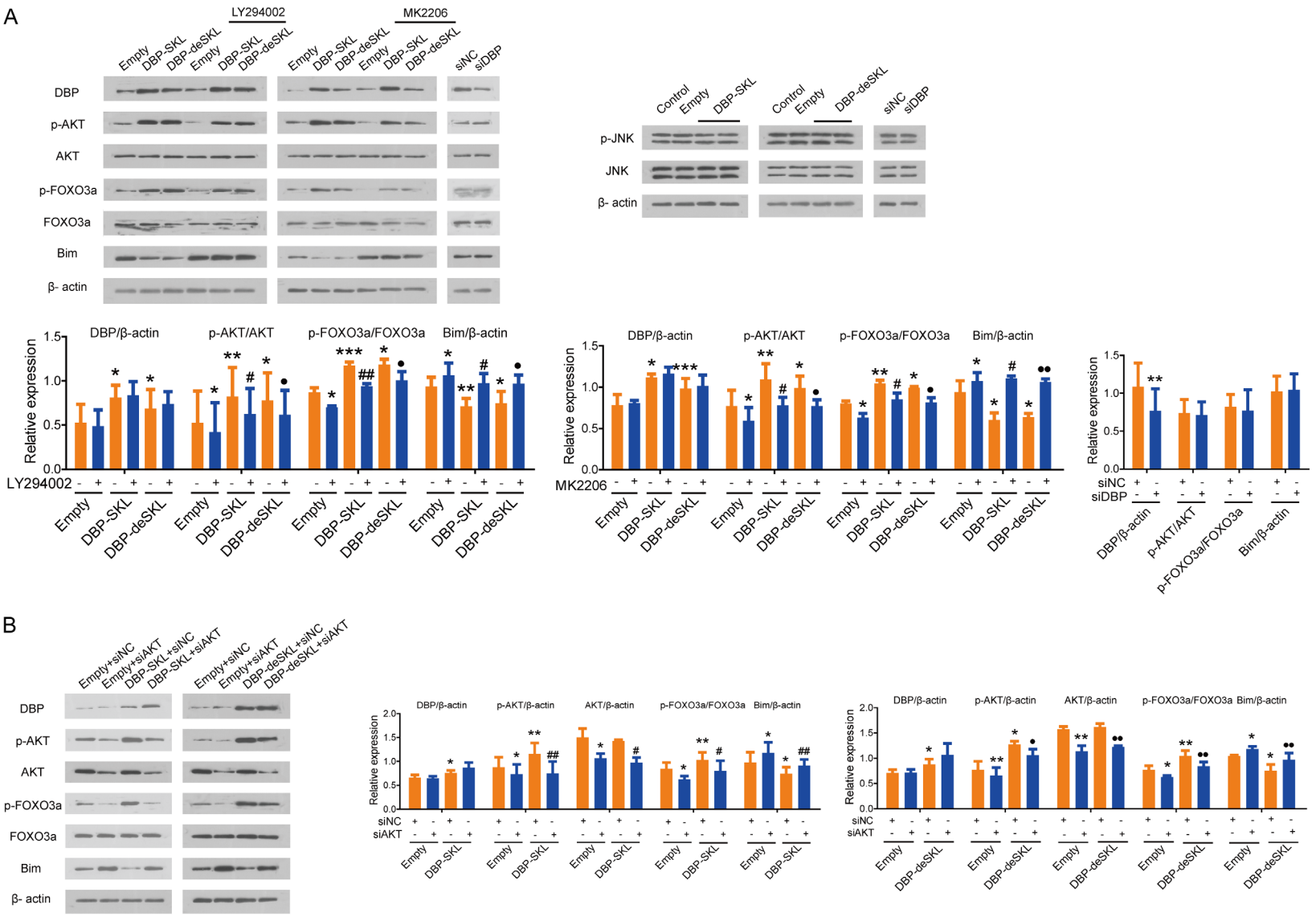
A
LY294002
MK2206
Empty
DBP-SKL
DBP-deSKL
siNC
siDBP
DBP
p-AKT
AKT
p-FOXO3a
FOXO3a
Bim
β- actin
Control
p-JNK
JNK
DBP/β-actin
p-AKT/AKT
p-FOXO3a/FOXO3a
Bim/β-actin
Relative expression
B
Empty+siNC
Empty+siAKT
DBP-SKL+siNC
DBP-SKL+siAKT
DBP-deSKL+siNC
DBP-deSKL+siAKT
AKT/β-actin

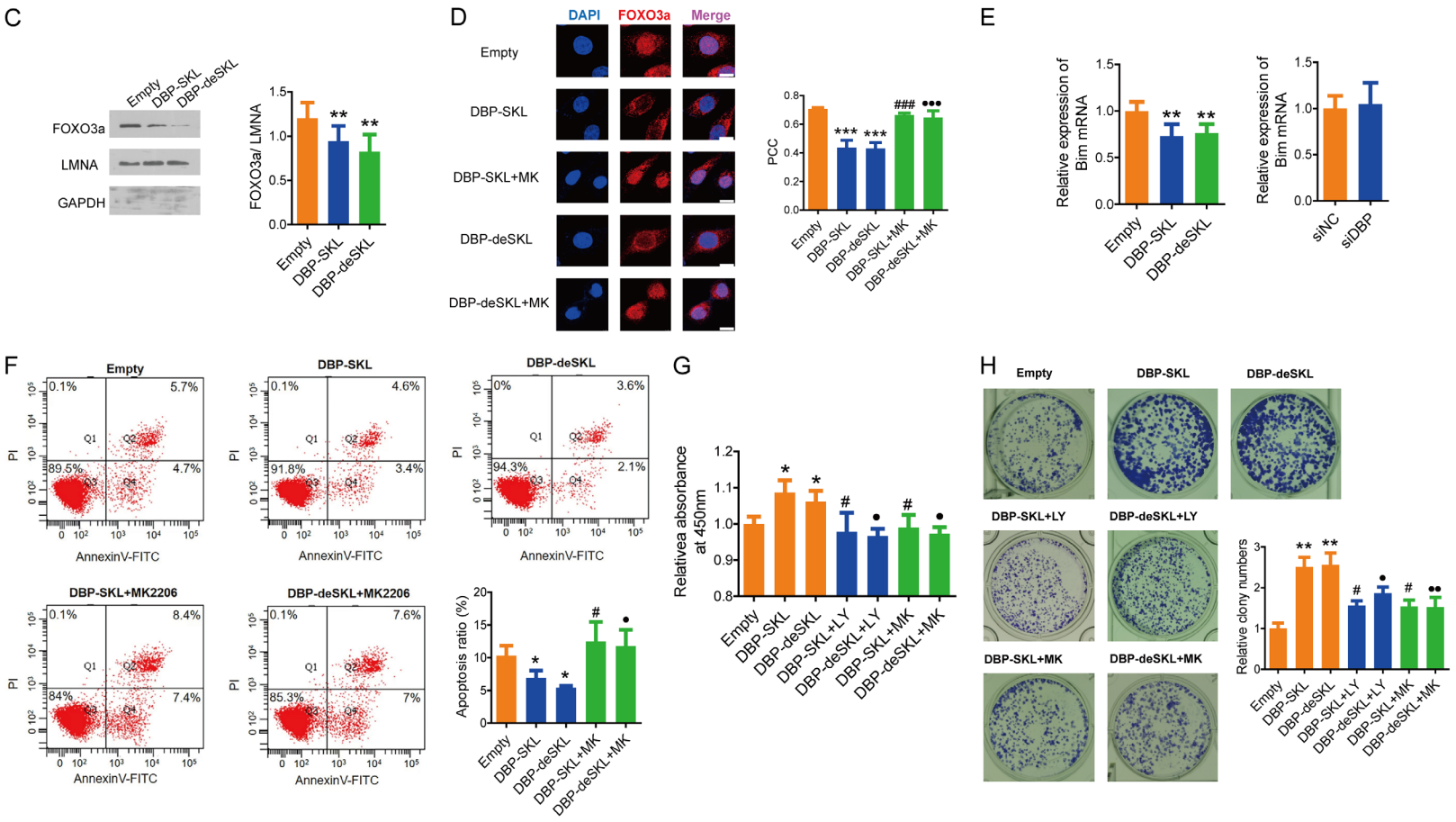

Figure 4. Cytosolic DBP promoted HepG2 cell proliferation via PI3K/AKT/FOXO3a/Bim pathway. A, B. Representative WB images of DBP, p-AKT, AKT, p-FOXO3a, FOXO3a, p-JNK, JNK, and Bim. β-actin served as a loading control. The quantitation of WB data was presented. C. Representative WB images of FOXO3a in the nuclear fraction. LAMN and GAPDH were nuclear and cytosolic markers, respectively. The quantitation of WB data was presented. D. The IF staining of FOXO3a (red), DAPI (blue), and their merge (purple). Quantitation of PCC data was presented. Scale bars = 10 μm. E. qRT-PCR to detect the expression of Bim. F. Apoptosis was assessed by flow cytometry with propidium iodide (PI)/Annexin V staining and the corresponding apoptosis ratio (%). Q2 region indicated late apoptotic cells with necrosis cells and mechanically damaged cells. Q4 indicated early apoptotic cells. G. Colony formation assay. H. CCK-8 assay. HepG2 cells were infected with control adenovirus (Empty), DBP-SKL, or DBP-deSKL. HepG2 cells were also treated with non-specific siRNA (siNC), DBP specific siRNA (siDBP), or AKT specific siRNA (siAKT). MK: MK2206, AKT inhibitor. LY: LY294002, PI3K inhibitor. Data were presented as mean ± SD. *P<0.05, **P<0.01 and ***P<0.001 vs. Empty group; #P<0.05, ##P<0.01 and ###P<0.001 vs. DBP-SKL group; •P<0.05, ••P<0.01 and •••P<0.001 vs. DBP-deSKL group.

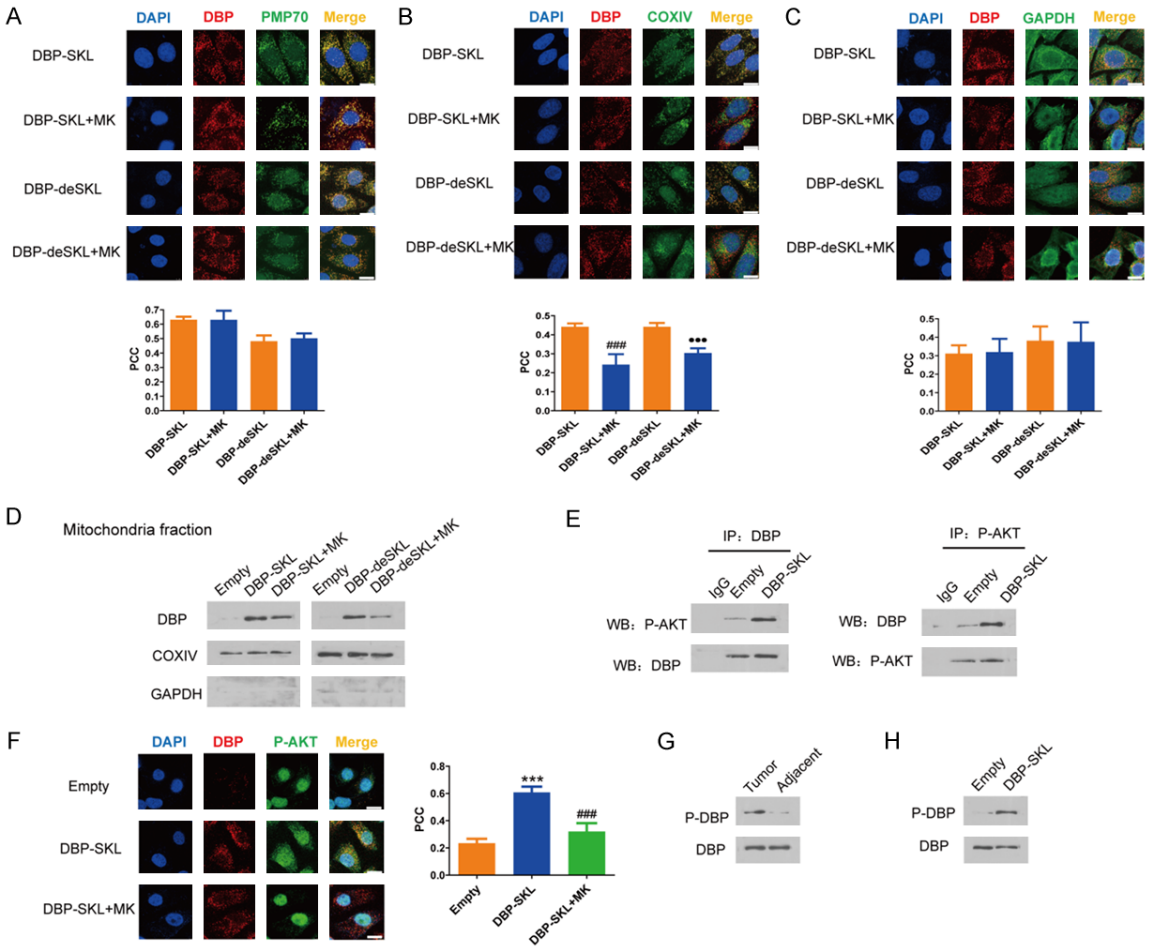

Figure 5. Mitochondrial localization of DBP was p-AKT-dependent. (A-C) The IF staining of DBP (red) in MK2206-treated DBP-SKL- and DBP-deSKL-expressing HepG2 cells. Cells were also co-stained with peroxisomal marker PMP70 (green) (A), mitochondrial marker COXIV (green) (B), and GAPDH (green) (C). Scale bars = 10 μm. PCC data were quantified. (D) WB of p-DBP in MK2206-treated mitochondria of DBP-SKL- or DBP-deSKL-overexpressing HepG2 cells. (E) CO-IP of DBP and p-Akt in DBP-SKL-expressing cells. (F) The IF staining of DBP (red) with p-AKT (green) in MK2206-treated DBP-SKL-expressing HepG2 cells. PCC data were quantified. Scale bar = 10 μm. (G) WB of p-DBP in tumor tissues and the adjacent liver tissues. (H) WB of p-DBP in DBP-SKL-overexpressing cells. HepG2 cells were infected with control adenovirus (Empty), DBP-SKL, or DBP-deSKL. MK: MK2206, AKT inhibitor. Data were presented as mean ± SD. ***P<0.001 vs. Empty group; ###P<0.001 vs. DBP-SKL group; •••P<0.001 vs. DBP-deSKL group.

ing group (n = 5; PCC_{deSKL} = 0.381±0.077, $PCC_{deSKL+MK2206}$ = 0.375±0.105, P>0.05) (**Figure 5C**), indicating that the cytosolic localization of DBP is not p-AKT dependent. MK2206 also decreased the DBP level in the mitochondrial fractions of the DBP-SKL- or DBP-deSKL-overexpressing cells (**Figure 5D**).

Furthermore, the CO-IP results suggested that p-AKT interacted with DBP in the DBP-SKL-overexpressing cells (**Figure 5E**). In addition, DBP and p-AKT were colocalized at higher level in the DBP-SKL group than in the empty vector group (n = 5; PCC_{Empty} = 0.2347±0.032, $PCC_{DBP-SKL}$ = 0.607±0.043; P<0.001), while MK2206 could attenuate this colocalization (n = 5; $PCC_{DBP-SKL+MK-2206}$ = 0.320±0.061, $P_{DBP-SKL+MK-2206\ vs.\ DBP-SKL}$<0.001, **Figure 5F**). Since antibody against the phosphorylated form of DBP was not available, we precipitated DBP with DBP antibody and then used a phosphorylated serine-specific antibody (p-Ser antibody) to determine the phosphorylated DBP level. The results showed that the level of phosphorylated DBP was not only significantly increased in tumor tissues compared to that in the paired adjacent tissues (**Figure 5G**), but also higher in the DBP-SKL group than in the Empty vector group (**Figure 5H**). This further confirmed that p-AKT phosphorylates DBP.

DBP overexpression promoted the production of glycogen and ATP in HepG2 cells via PI3K/AKT/GSK3β signaling pathway

To investigate whether the activation of AKT was accompanied by the phosphorylation of GSK3β (Ser9), a substrate of p-AKT [14], we examined the p-GSK3β (Ser9) level in HepG2 cells by WB and found that p-GSK3β (Ser9) level was not significantly affected by DBP knockdown (P>0.05; **Figure 6A**); however, overexpression of DBP-SKL or DBP-deSKL increased p-GSK3β (Ser9) level (P<0.05; **Figure 6A**), which could be abolished by LY294002, MK2206, and siAKT (P<0.05; **Figure 6A**, **6B**).

Importantly, we examined the effect of DBP-SKL or DBP-deSKL overexpression on glycogen production as p-GSK3β (Ser9) is a key enzyme in glycogen synthesis (P<0.05; **Figure 6C**) as well as on glucose uptake (P<0.05; **Figure 6D**) in HepG2 cells. As expected, the glycogen level was higher in HCC tumor tissues than in the paired adjacent tissues (**Figure 6E**).

It has been reported that GSK3β phosphorylation at serine 9 can relieve the inhibition of mitochondrial respiratory chain complex III activity in mitochondria, thus promoting ATP production [15]. Consistently, we found that overexpression of DBP-SKL or DBP-deSKL significantly increased p-GSK3β (Ser9) level in the mitochondrial fractions of HepG2 cells (P<0.05; **Figure 6F**). In addition, a higher level of colocalization between p-GSK3β (Ser9) and mitochondria marker COXIV was observed in HepG2 cells overexpressing DBP-SKL (n = 5; PCC = 0.426±0.048; P<0.001) and DBP-deSKL (n = 5; PCC = 0.413±0.009; P<0.001) compared to that in empty vector-expressing cells group (n = 5; PCC = 0.185±0.025), while MK2206 could attenuate this effect in DBP-SKL+MK group (n = 5; PCC = 0.184±0.056; P<0.01) and DBP-deSKL+MK group (n = 5; PCC = 0.231±0.043; P<0.001) (**Figure 6G**).

We also found that, along with the increased mitochondrial p-GSK3β (Ser9) level, the activity of mitochondrial respiratory chain complex III (P<0.05; **Figure 6H**) and the ATP level (P<0.01; **Figure 6I**) were increased in DBP-SKL- and DBP-deSKL-overexpressing HepG2 cells, which was abolished by MK2206 (P<0.05; **Figure 6H**, **6I**), suggesting that the cytosolic DBP could upregulate ATP levels via activating mitochondrial respiratory chain complex III through modulating p-GSK3β (Ser9) level.

Discussion

DBP is the key enzyme of fatty acid peroxisomal β-oxidation that participates in the β-oxidation of long- and branched-chain fatty acids, bile acid biosynthesis, as well as sterol metabolism [16]. Over the last decade, accumulating evidence has indicated the involvement of peroxisomal DBP in the initiation and progression of various tumors. For example, the upregulation of DBP was associated with the cell proliferation in prostate cancer [3], liver cancer [6], and colon cancer [17], while DBP plays an inhibitory role in adrenocortical carcinoma [18] and ovarian epithelial carcinoma [4]. In addition, the downregulated expression of DBP was associated with immune dysfunction in non-small cell lung cancer [19]. Our previous studies have shown that DBP overexpression in HepG2 cells promotes cell proliferation by inactivating estradiol activity but activating several oncogenic molecules, including PI3K, AKT, STAT3, Cyclin D1, and PCNA. Herein, we further confirmed that DBP is highly expressed in HCC tumor tissues and is a cancer promoting factor in HCC. In addition, we proved that the highly expressed DBP was located in the peroxisome, mitochondrion, and cytosol of HCC tissue and cell line and that cytosolic DBP promoted the growth of xenograft tumor by activating the PI3K/AKT pathway.

The PI3K/AKT signaling pathway is well known to play an important role in cell proliferation, apoptosis, and inflammation [20]. Consistently, our previous studies have shown that DBP overexpression activates PI3K/AKT to promote the proliferation of HCC cells. This study further demonstrated that PI3K was activated by the cytosolic DBP, which in turn induced the phosphorylation of AKT and the subsequent phosphorylation of FOXO3a, GSK3β, and DBP, thereby leading to metabolic alterations. While a variety of growth factors including fibroblast growth factor (FGF), vascular endothelial growth factor (VEGF), and insulin-like growth factor-1 (IGF-1), can activate PI3K through the activation of receptor tyrosine kinase (RTK), how DBP activates the PI3K/AKT signaling pathway is still unclear.

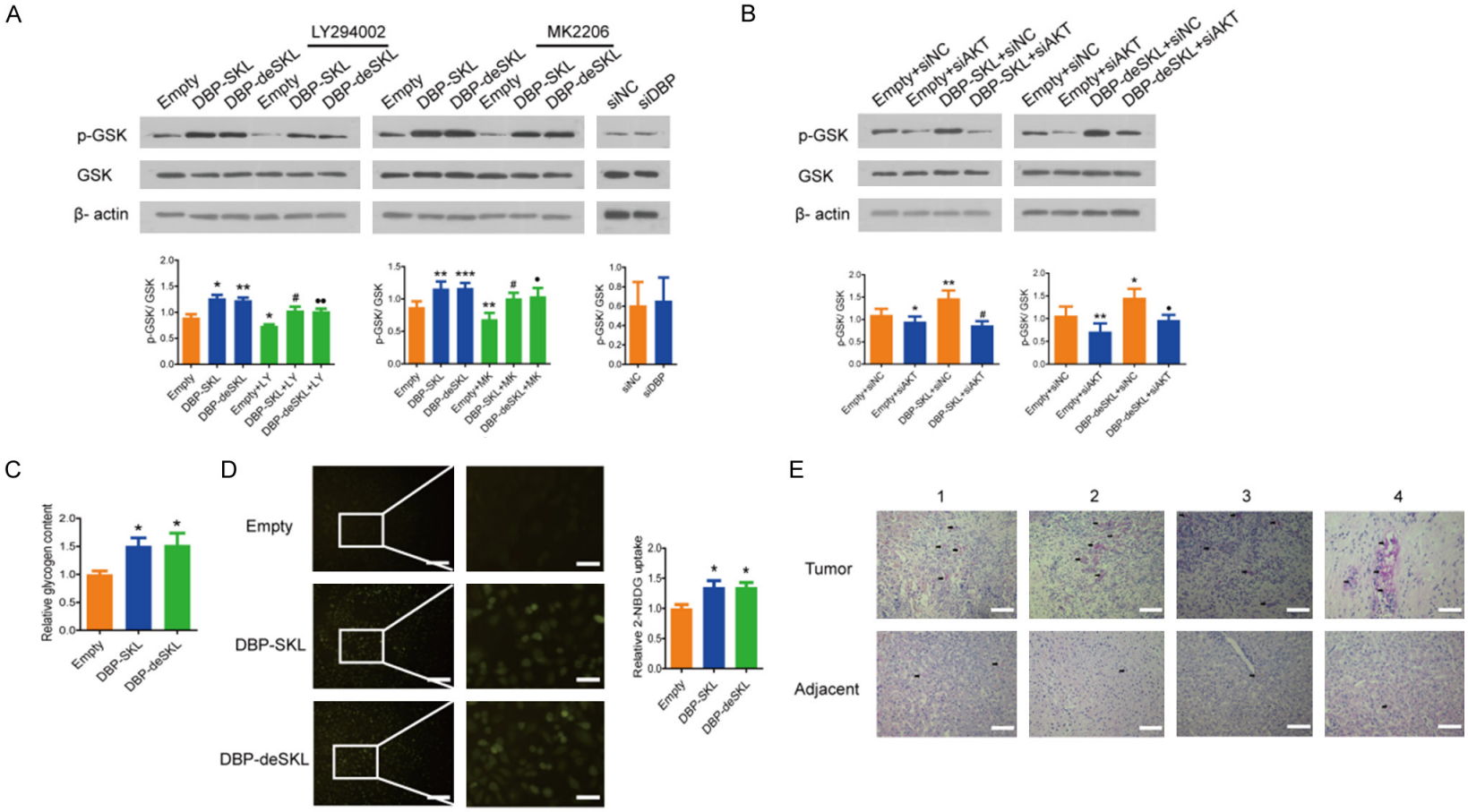
A
LY294002
MK2206
Empty
DBP-SKL
DBP-deSKL
siNC
siDBP
p-GSK
GSK
β- actin
p-GSK/ GSK
B
Empty+siNC
Empty+siAKT
DBP-SKL+siNC
DBP-SKL+siAKT
DBP-deSKL+siNC
DBP-deSKL+siAKT
C
Relative glycogen content
D
Relative 2-NBDG uptake
E
1
2
3
4
Tumor
Adjacent

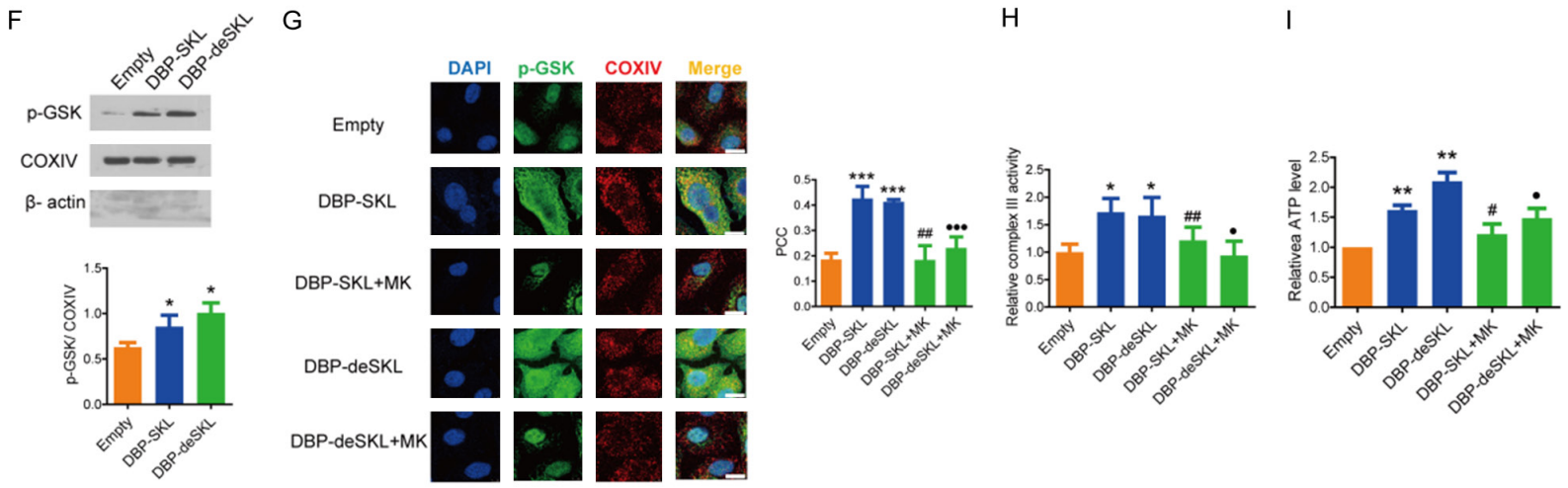

Figure 6. Cytosolic DBP regulated the production of glycogen and ATP in HepG2 cells via PI3K/AKT/GSK3β signaling pathway. A, B. WB of p-GSK3β and GSK3β. β-actin: loading control. Data were quantified. C. Glycogen levels in the indicated cells. D. Glucose uptake as indicated by 2-NBDG fluorescence intensity in the treated cells. Scale bar (left) = 100 μm, scale bar (right) = 30 μm. E. Glycogen staining by PAS in tumors and the adjacent liver tissues of HCC patients (n = 4). PAS-positive staining (magenta) was marked by arrows. Scale bars = 100 μm. F. WB of p-GSK3β in the mitochondrial fraction of cells. COXIV and β-actin: mitochondrial and cytosolic markers, respectively. Data were quantified. G. The IF staining of p-GSK3β (green), mitochondrial COXIV (red), and their merge (yellow). PCC data were quantified. Scale bars = 10 μm. H. The enzymatic activity of mitochondrial respiratory chain complex III in the treated cells. I. ATP levels in the treated cells. HepG2 cells were infected with control adenovirus (Empty), DBP-SKL, or DBP-deSKL. HepG2 cells were also treated with non-specific siRNA (siNC), DBP specific siRNA (siDBP), AKT specific siRNA (siAKT). MK: MK2206, AKT inhibitor. Data were presented as mean ± SD. *P<0.05, **P<0.01 and ***P<0.001 vs. Empty group; #P<0.05, ##P<0.01 vs. DBP-SKL group; •P<0.05, ••P<0.01 and •••P<0.001 vs. DBP-deSKL group.

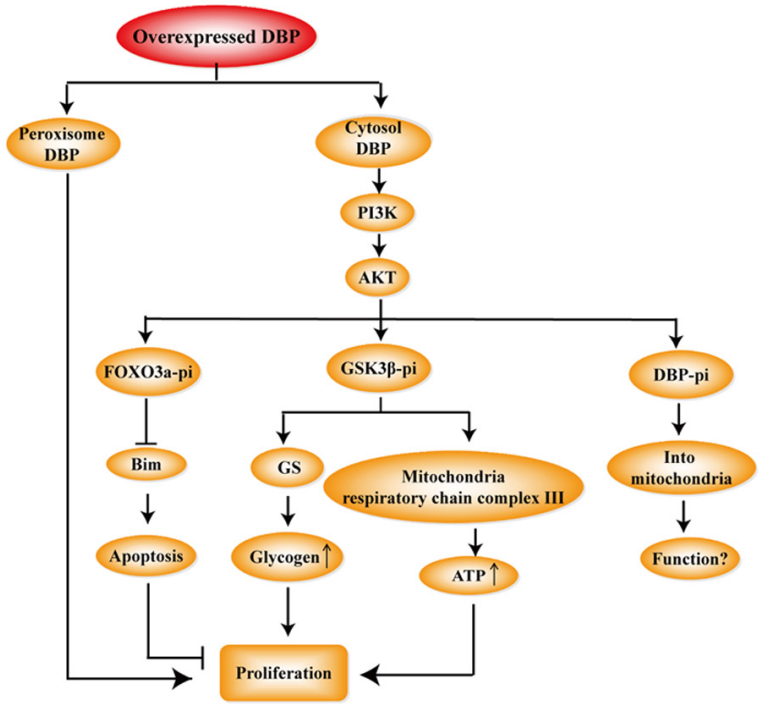

Figure 7. Diagram of the role of DBP upregulation in HCC cell proliferation. Cytosolic DBP activates the PI3K/Akt signaling pathway, which induces the phosphorylation of FOXO3a, GSK3β, and DBP. Phosphorylated DBP can enter mitochondria, but its role is unknown. Phosphorylated FOXO3a and GSK3β promote the proliferation of HCC cells by downregulating Bim to inhibit cell apoptosis and activating GS and respiratory chain complex III to elevate glycogen and ATP levels, respectively. DBP in peroxisome is also necessary for HCC cell proliferation, independent of the PI3K/Akt signaling pathway.

Phosphorylation of FOXO3a by AKT inactivates its transcriptional activity, leading to the transcriptional suppression of Bim, a member of the Bcl-2 apoptotic protein family, which in turn inhibits apoptosis [21]. In this study, we observed that overexpression of cytosolic DBP promotes the proliferation of HCC cells by suppressing apoptosis via the AKT-FOXO3a-Bim pathway. It is known that AKT inhibits the activity of GSK3β by phosphorylating GSK3β at serine 9. GSK3β regulates many cellular processes, including proliferation and energy metabolism [22]. AKT-phosphorylated GSK3β (Ser9) promotes cell proliferation by inducing cyclin D1 expression [23, 24]. The present study also found that overexpression of cytosolic DBP elevated AKT-phosphorylated GSK3β (Ser9) level, suggesting that the AKT/GSK3β pathway might be involved in HCC cell proliferation.

Glycogen synthase (GS) is the rate-limiting enzyme in glycogen synthesis in the liver. GSK3β catalyzes the phosphorylation of GS to reduces its activity, thereby leading to a reduced glycogen synthesis. In this study, we revealed that the overexpression of cytosolic DBP enhanced glycogen synthesis and glucose uptake through AKT-induced GSK3β inactivation. These results were consistent with the report that glycogen synthesis was increased in hepatocellular carcinoma, and p-GSK3β (Ser9) could also increase glucose uptake [25].

Furthermore, GSK3β can significantly inhibit the activity of complex I, II, III, and IV in the respiratory chain and the conversion of ADP to ATP, resulting in an attenuated ATP production, while phosphorylated GSK3β (Ser9) can relieve the above inhibition [15]. In our study, we found that AKT-stimulated p-GSK3β (Ser9) was accumulated in mitochondria, and the activity of the respiratory chain complex III and ATP level were upregulated in DBP-overexpressing cells, suggesting that the overexpressed cytosolic DBP could provide the energy for elevated cell proliferation by regulating p-GSK3β (Ser9) level.

In conclusion (**Figure 7**), our study was the first to demonstrate an upregulation of DBP in the peroxisome, cytosol, and mitochondrion of HCC. Importantly, DBP in the peroxisome has an indispensable role in the proliferation of HCC, while DBP in the cytosol can activate PI3K/AKT to promote cell growth by suppressing apoptosis via AKT/FOXO3a/Bim cascade and increase the synthesis of glycogen and ATP via AKT/GSK3β. Notably, the AKT-phosphorylated DBP was translocated into mitochondria, the significance of which needs further exploration.

Acknowledgements

This study was supported by the Health Commission of Hebei Province (20180888)

and the National Natural Science Foundation of China (81800742).

Disclosure of conflict of interest

None.

Address correspondence to: Ling-Ling Jiang, Ministry of Education Key Laboratory of Neural and Vascular Biology, Department of Biochemistry and Molecular Biology, Hebei Medical University, No. 361, Zhongshan East Road, Shijiazhuang 050017, Hebei, China. E-mail: jllxwlw@163.com

References

[1] Mindnich R, Möller G and Adamski J. The role of 17 beta-hydroxysteroid dehydrogenases. Mol Cell Endocrinol 2004; 218: 7-20.

[2] Verheijden S, Bottelbergs A, Krysko O, Krysko DV, Beckers L, De Munter S, Van Veldhoven PP, Wyns S, Kulik W, Nave KA, Ramer MS, Carmeliet P, Kassmann CM and Baes M. Peroxisomal multifunctional protein-2 deficiency causes neuroinflammation and degeneration of Purkinje cells independent of very long chain fatty acid accumulation. Neurobiol Dis 2013; 58: 258-269.

[3] Rasiah KK, Gardiner-Garden M, Padilla EJ, Möller G, Kench JG, Alles MC, Eggleton SA, Stricker PD, Adamski J, Sutherland RL, Henshall SM and Hayes VM. HSD17B4 overexpression, an independent biomarker of poor patient outcome in prostate cancer. Mol Cell Endocrinol 2009; 301: 89-96.

[4] Motohara K, Tashiro H, Taura Y, Ohba T and Katabuchi H. Immunohistochemical analysis of 17β-hydroxysteroid dehydrogenase isozymes in human ovarian surface epithelium and epithelial ovarian carcinoma. Med Mol Morphol 2010; 43: 197-203.

[5] Lu X, Ma P, Shi Y, Yao M, Hou L, Zhang P and Jiang L. NF-κB increased expression of 17β-hydroxysteroid dehydrogenase 4 promotes HepG2 proliferation via inactivating estradiol. Mol Cell Endocrinol 2015; 401: 1-11.

[6] Lu X, Kong L, Wang X, Liu W, Ma P and Jiang L. 17β-hydroxysteroid dehydrogenase 4 induces liver cancer proliferation-associated genes via STAT3 activation. Oncol Rep 2019; 41: 2009-2019.

[7] Bookout AL and Mangelsdorf DJ. Quantitative real-time PCR protocol for analysis of nuclear receptor signaling pathways. Nucl Recept Signal 2003; 1: e012.

[8] Fishbein MC, Wang T, Matijasevic M, Hong L and Apple FS. Myocardial tissue troponins T and I. An immunohistochemical study in experimental models of myocardial ischemia. Cardiovasc Pathol 2003; 12: 65-71.

[9] Huang H, Shao Q, Qu C, Yang T, Dwyer T and Liu G. Coordinated interaction of Down syndrome cell adhesion molecule and deleted in colorectal cancer with dynamic TUBB3 mediates Netrin-1-induced axon branching. Neuroscience 2015; 293: 109-122.

[10] Li GB, Zhang XL, Yuan L, Jiao QQ, Liu DJ and Liu J. Protein phosphatase magnesium-dependent 1δ (PPM1D) mRNA expression is a prognosis marker for hepatocellular carcinoma. PLoS One 2013; 8: e60775.

[11] Lu X, Ma P, Kong L, Wang X, Wang Y and Jiang L. Vitamin K2 inhibits hepatocellular carcinoma cell proliferation by binding to 17β-hydroxysteroid dehydrogenase 4. Front Oncol 2021; 11: 757603.

[12] Shukla S, Shukla M, Maclennan GT, Fu P and Gupta S. Deregulation of FOXO3A during prostate cancer progression. Int J Oncol 2009; 34: 1613-1620.

[13] Shukla S, Bhaskaran N, Maclennan GT and Gupta S. Deregulation of Fox03a accelerates prostate cancer progression in TRAMP mice. Prostate 2013; 73: 1507-1517.

[14] Shieh JM, Wu HT, Cheng KC and Cheng JT. Melatonin ameliorates high fat diet-induced diabetes and stimulates glycogen synthesis via a PKCzeta-Akt-GSK3beta pathway in hepatic cells. J Pineal Res 2009; 47: 339-344.

[15] Yang K, Chen Z, Gao J, Shi W, Li L, Jiang S, Hu H, Liu Z, Xu D and Wu L. The key roles of GSK-3β in regulating mitochondrial activity. Cell Physiol Biochem 2017; 44: 1445-1459.

[16] Poutanen M, Isomaa V, Peltoketo H and Vihko R. Regulation of oestrogen action: role of 17 beta-hydroxysteroid dehydrogenases. Ann Med 1995; 27: 675-682.

[17] Frasinyuk MS, Zhang W, Wyrebek P, Yu T, Xu X, Sviripa VM, Bondarenko SP, Xie Y, Ngo HX, Morris AJ, Mohler JL, Fiandalo MV, Watt DS and Liu C. Developing antineoplastic agents that target peroxisomal enzymes: cytisine-linked isoflavonoids as inhibitors of hydroxysteroid 17-beta-dehydrogenase-4 (HSD17B4). Org Biomol Chem 2017; 15: 7623-7629.

[18] Ding G, Liu S, Ding Q and Feng C. Overexpression of HSD17B4 exerts tumor suppressive function in adrenocortical carcinoma and is not associated with hormone excess. Oncotarget 2017; 8: 114736-114745.

[19] Zhang X, Yang H, Zhang J, Gao F and Dai L. HSD17B4, ACAA1, and PXMP4 in peroxisome pathway are down-regulated and have clinical significance in non-small cell lung cancer. Front Genet 2020; 11: 273.

[20] Sun Y, Zhao Y, Wang X, Zhao L, Li W, Ding Y, Kong L, Guo Q and Lu N. Wogonoside prevents

colitis-associated colorectal carcinogenesis and colon cancer progression in inflammation-related microenvironment via inhibiting NF-κB activation through PI3K/Akt pathway. Oncotarget 2016; 7: 34300-34315.

[21] Fasano C, Disciglio V, Bertora S, Lepore Signorile M and Simone C. FOXO3a from the nucleus to the mitochondria: a round trip in cellular stress response. Cells 2019; 8: 110.

[22] Shakoori A, Ougolkov A, Yu ZW, Zhang B, Modarressi MH, Billadeau DD, Mai M, Takahashi Y and Minamoto T. Deregulated GSK-3beta activity in colorectal cancer: its association with tumor cell survival and proliferation. Biochem Biophys Res Commun 2005; 334: 1365-1373.

[23] Chen Y, Liu X, Wang H, Liu S, Hu N and Li X. Akt regulated phosphorylation of GSK-3β/cyclin D1, p21 and p27 contributes to cell proliferation through cell cycle progression from G1 to S/G2M phase in low-dose arsenite exposed HaCat cells. Front Pharmacol 2019; 10: 1176.

[24] Takahashi-Yanaga F and Sasaguri T. GSK-3beta regulates cyclin D1 expression: a new target for chemotherapy. Cell Signal 2008; 20: 581-589.

[25] Chen XY, Li DF, Han JC, Wang B, Dong ZP, Yu LN, Pan ZH, Qu CJ, Chen Y, Sun SG and Zheng QS. Reprogramming induced by isoliquiritigenin diminishes melanoma cachexia through mTORC2-AKT-GSK3β signaling. Oncotarget 2017; 8: 34565-34575.